Nanowire bundles

DOI: 10.1002/smll.200700164

Nanomechanical Investigation of $Mo_6S_{9-x}I_x$ Nanowire Bundles**

*Andras Kis, Gábor Csanyi, Daniel Vrbanic, Ales Mrzel, Dragan Mihailovic, Andrezj Kulik, and Lázsló Forró**

A wide variety of anisotropic layered materials are capable of forming interesting nanostructures such as nanotubes and nanoparticles with unique properties and a wide range of potential applications. Carbon nanotubes are the earliest example of such materials.[1] Similar nanostructures, such as boron nitride nanotubes,[2] tungsten disulphide and molybdenum disulphide fullerene-like nanoparticles and tubular structures,[3,4] are well-known representatives of a large group of inorganic nanotubes. They are a viable alternative to carbon nanotubes in many potential fields of applications, especially in nanoscale electronics. Their bandgaps are functions of the diameter so they can easily be produced in large quantities and with a narrow distribution of electronic properties. This is in stark contrast to carbon nanotubes, which are always produced as a mixture of metallic, p- and n-type semiconducting tubes.

Particularly interesting are the recently discovered subnanometer-diameter one-dimensional (1D) materials such as MoS_xI_y nanotubes[5] and $Mo_6S_{9-x}I_x$ nanowires.[6] From a structural point of view these materials are similar to transition-metal chalcogenide compounds, the Chevrel phases,[7] and cannot be thought of as curled-up sheets of bulk, layered materials. They are functionally similar to carbon nanotubes with excellent field-emission properties,[8] extremely weak mechanical intertube coupling,[9] an anomalously large paramagnetic susceptibility,[10] and interesting electronic properties.[11–13] The structure of two of the newly discovered materials of nanowires, $Mo_6S_3I_6$ and $Mo_6S_{4.5}I_{4.5}$, are shown in Figure 1. X-ray diffraction (XRD), extended X-ray absorption fine-structure analysis (EXAFS)[14] and X-ray powder diffraction[15] measurements indicate that both types of nanowire share the same structure, with individual nanowires composed of Mo_6 octahedral clusters separated by bridging anions (S). The surface of every wire is dressed with six additional anions (S and I, depending on the stoichiometry).[14] The detailed structure has recently been determined using high-resolution transmission electron microscopy (HRTEM) techniques.[16] Varying ratios of S and I atomic species are expected to modify the van der Waals interaction between individual wires. Central sites (C) are expected to have low or zero atomic populations.

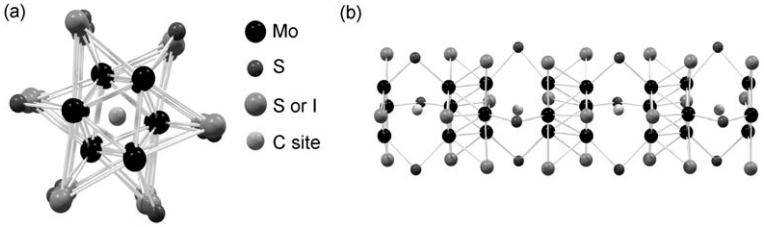

Figure 1. The structure of $Mo_6S_{9-x}I$ nanowire bundles. a) The model structure viewed from the direction perpendicular to the nanowire axis. b) The model structure shown parallel to the nanowire axis. Mo_6 octahedra decorated with sulfur and iodine atoms in varying ratios, depending on the stoichiometry, are connected by bridging sulfur atoms. Central sites (C) have low or zero atomic populations.

The materials are monodisperse with individual nanowire strands having a diameter of 0.94 nm and identical electronic properties, determined by their stoichiometry, described by the formula $Mo_6S_{9-x}I_x$. The stoichiometry itself is adjusted by the weight ratios of elemental Mo, S, and I in the starting synthesis material.[6] These nanowires could be easily functionalized due to their sulfur-based chemistry, which makes them interesting for biological applications and sensor fabrication. $Mo_6S_{9-x}I_x$ nanowires can be dispersed in a wide range of organic solvents including isopropyl alcohol, dimethylformamide, chloroform and, in the case of $Mo_6S_3I_6$, water.[6,17] Different degrees of dilution yield nanowire bundles with different diameters, with higher degrees of dilution resulting in thinner nanowire bundles. This provides a very practical means to control bundle diameter for future studies and applications. The easy dispersion of $Mo_6S_3I_6$ and $Mo_6S_{4.5}I_{4.5}$ also makes these materials attractive for composite fabrication.

Preliminary results show that these two materials are characterized by electrical conductivity above 10 $S\,m^{-1}$, reasonably good thermal stability with decomposition temperatures in air exceeding 200 °C, and a very low friction coefficient of 0.03.[6] Low values of the friction coefficient are typical of nanostructures related to layered materials such as

[*] Dr. A. Kis, A. Kulik, Prof. L. Forró
Institut de la Physique de la Matière Complexe
EPFL, 1015 Lausanne (Switzerland)
Fax: (+41) 216-934-470
E-mail: laszlo.forro@epfl.ch
Dr. G. Csanyi
Cavendish Laboratory, University of Cambridge
Cambridge CB3 oHE (UK)
D. Vrbanic, Dr. A. Mrzel, Prof. D. Mihailovic
Jozef Stefan Institute
Jamova 39, 1000 Ljubljana (Slovenia)

[**] We would like to thank G. Beney for polishing the Al_2O_3 membranes and J.-P. Salvetat for interesting discussions. The access to electron microscopes was kindly provided by the Centre Interdépartmental de Microscopie Electronique (CIME) at the EPFL. Computations were carried out on the Cambridge-Cranfield High Performance Computer Facility. This work was in part supported by the European TMR network "Nanotemp".

Supporting information for this article is available on the WWW under http://www.small-journal.com or from the author.

MoS_2 and graphite, characterized by weak van der Waals interactions between individual layers that allows easy, low-strength shearing.[18] Carbon and MoS_2 nanotube bundles are the best-known examples of such nanomaterials, exhibiting very low resistance to intertube sliding,[9,19] which makes them interesting for future nanoscale mechanical systems, such as bearings. The ease with which $Mo_6S_{9-x}I_x$ nanowire bundles can be dispersed indicates that this material could also exhibit low resistance to sliding. In addition, it gives us the opportunity to study the subtle effect that stoichiometry variations might have on the strength of interaction between individual wires comprising the bundle. The most convenient way of studying the interaction between wires is by measuring the mechanical properties of nanowire bundles. In particular, the shear modulus of bundles would give a direct measure of the strength of interaction between individual wires comprising the bundle.

Accompanying the nanomechanical measurements, a theoretical prediction of the Young's modulus of $Mo_6S_{9-x}I_x$ nanowires with $x=6$ was made using a model based on density-functional theory (DFT) with full internal relaxation. The structure of $Mo_6S_{9-x}I_x$ nanowires based on XRD and X-ray absorption measurements[14] was used as a starting point for determining energy-optimized configurations using DFT calculations, as shown in Figure 1.

We used the CASTEP[20] plane-wave pseudopotential simulation package; the electron correlation was described with the PBE-gradient-corrected functional[21] and the orbital occupancies were optimized with ensemble DFT (EDFT).[22] The Young's modulus of the experimental structure is about 45 GPa. Given that we are dealing with covalently bonded tubular structures such a small value is surprising and its origin can be traced back to the fact that the clusters of six Mo atoms move rigidly under stress, whereas the S bridges connecting them are very flexible and to first order only bond angles are stressed. Noting that the occupancy of the C site (Figure 1) situated on the nanowire axis near the bridge sites would considerably increase the stiffness, we explored various hypothetical structures in which Mo, S, and I atoms were placed there, even though there is no direct experimental evidence for the presence of any atoms there. The Young's modulus of the resulting structures more than doubled in the case of S or I at the C site. As discussed below, this still falls far short of the experimentally obtained Young's modulus. This result is in apparent agreement with recent calculations by Vilfan et al. and Yang et al.[12,13] Due to the difficulty of describing van der Waals interactions within DFT, no attempt was made to simulate a nanowire bundle or to calculate the shear modulus. Atomistic models or molecular dynamics simulations, successful in simulating shearing between layers of multi-walled carbon nanotubes,[23] could in principle be applied to $Mo_6S_{9-x}I_x$ nanowires but a suitable atomic potential for this system would have to be developed first.

HRTEM images reveal well-ordered structures in the form of bundles (Figure 2a and b) with individual nanowire diameters of 0.94 nm.[6] These bundles can be easily dispersed in a wide range of organic and polar solvents using ultrasound. Different dispersion concentrations yield a varying bundle-diameter distribution, with the average bundle diameter decreasing on greater dilution.[17]

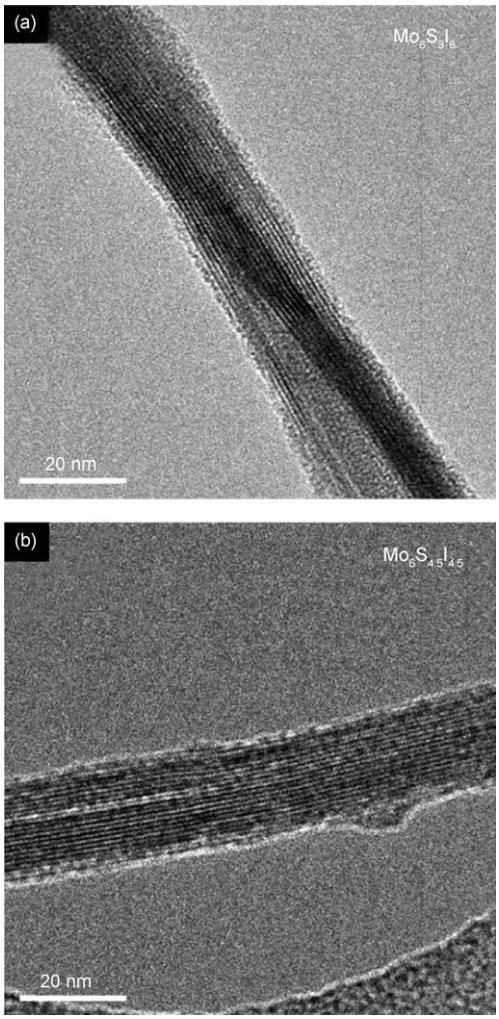

Figure 2. TEM images of well-aligned bundles composed of individual $Mo_6S_{9-x}I_x$ nanowires. a) TEM image of a bundle of $Mo_6S_3I_6$ nanowires. b) TEM image of a bundle of $Mo_6S_{4.5}I_{4.5}$ nanowires.

Nanomechanical measurements are carried out using the tip of an atomic force microscope (AFM) to elastically deform suspended nanowire bundles in order to determine their shear modulus G, corresponding to sliding between individual nanowires comprising the bundle. This well-established method was previously applied to carbon-nanotube bundles,[19] multi-walled nanotubes,[24,25] irradiated carbon nanotubes[26] and cytoskeletal filaments (microtubules).[27]

$Mo_6S_{9-x}I_x$ nanowires are dispersed in isopropyl alcohol and deposited on the surface of a polished alumina ultrafiltration membrane. Bundles consisting of individual nanowires occasionally lie over pores in the membrane surface (Figure 3a). They are firmly held in place by surface adhesion on supported portions, as confirmed by continuous AFM imaging. This allows us to apply the clamped-beam model for describing nanowire-bundle deformation. In the case of weak substrate adhesion, sliding prevents stable imaging and eliminates these bundles from the rest of the

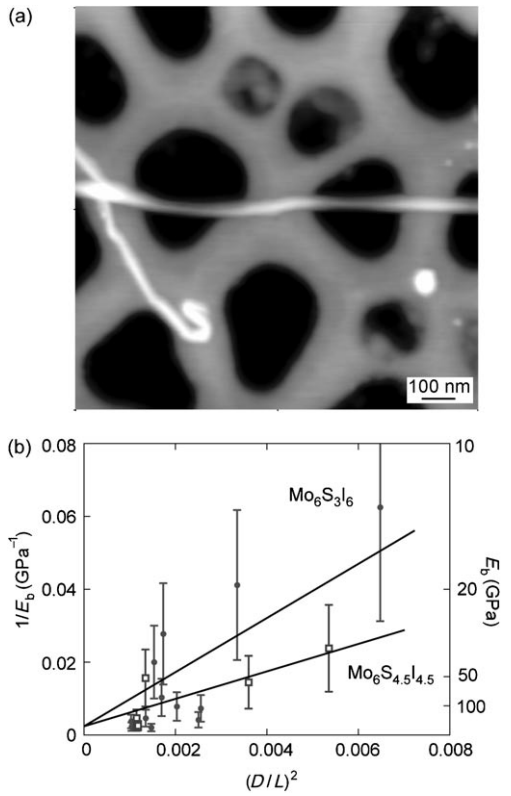

Figure 3. Nanomechanical measurements. a) AFM image of a bundle of $Mo_6S_{4.5}I_{4.5}$ nanowires deposited on Al_2O_3. The bundle is deformed during AFM imaging in contact mode, which allows us to determine E_b of the bundle. b) The plot of E_b measured for 13 different MoS_2 bundles as a function of bundle geometry (total external diameter D divided by the length of the suspended bundle). The value of E_b varies due to intertube shearing. The shear modulus G can be obtained from the slope of the linear fit. E_Y describes the resistance of the entire bundle to stretching, while G describes sliding between individual nanowires comprising the bundle.

measurement. After a suitable nanowire bundle had been found a series of contact-mode AFM images is taken under increasing load, with every image corresponding to the topography of the surface under a given normal load.

Geometrical parameters, the rope's diameter (D), suspended length (L), and vertical deflection in the middle (δ) are all determined from AFM images similar to the one shown in Figure 3a using image-analysis software. Due to convolution of the rope with the AFM tip, the rope appears broadened and we therefore use the rope's height as an accurate measure of its diameter. Extracted line scans across the bundle reveal its deformation and vertical deflection. For the range of forces used for imaging we did not observe any change in bundle height on supported portions, allowing us to neglect the effects of bundle compression and indentation. The effect of cantilever deflection is taken into account by measuring the height difference between the hard substrate (Al_2O_3 membrane) and the suspended bundle. In more conventional approaches based on the acquisition of force–distance curves in precise locations[28] this is usually done by subtracting reference curves acquired on hard substrates.

For the range of applied normal force the midpoint deflection consists of bending (δ_B) and shearing deformation (δ_S). The total deformation can be calculated using the unit-load method[29] and is given by the following linear relationship:

$$\delta = \delta_B + \delta_S = \frac{FL^3}{192E_Y I} + f_S \frac{FL}{4GA} = \frac{FL^3}{192E_b I} \quad (1)$$

where F is the applied normal force, L the suspended length of the bundle, E_Y the Young's modulus, I the second moment of the area, fs the shape factor (equal to 10/9 for a cylindrical beam), G the shear modulus, and D the external diameter of the nanowire bundle. Capillary force and adhesion are constant during the measurement and result in additional constant force acting on the wires. E_b is calculated from the slope of the linear fit as a result of a single bending experiment and equals the Young's modulus when the influence of shearing can be neglected, ideally for isolated nanowires. Equation (1) can be simplified and E_b expressed as:

$$\frac{1}{E_b} = \frac{1}{E_Y} + \frac{10}{3G}\frac{D^2}{L^2} \quad (2)$$

Both $Mo_6S_3I_6$ and $Mo_6S_{4.5}I_{4.5}$ bundles are composed of identical single nanowires, all with a diameter of 0.94 nm, while the bundles' external diameter changes with the number of nanowires comprising it. E_b describes the resistance of the entire bundle to bending, E_Y the resistance of nanowires to stretching, while G describes sliding between individual nanowires forming the bundle (Figure 2a and b). In the case of anisotropic materials such as $Mo_6S_3I_6$ and $Mo_6S_{4.5}I_{4.5}$ bundles, the relevant material constants, E_Y and G can be extrapolated by measuring the E_b of an ensemble of bundles with different diameter-to-length ratios. Varying the external diameter of bundles that correspond to a different number of bundled-up nanowires effectively varies the relative weights of shearing to stretching in the total mechanical response.

The variation of $1/E_b$ plotted as a function of $(D/L)^2$ for several $Mo_6S_3I_6$ and $Mo_6S_{4.5}I_{4.5}$ bundles with external diameters in the 10–25-nm range are shown in Figure 3. From fits to Equation 2, values of the shear modulus of $Mo_6S_3I_6$ nanowires of $G = 450 \pm 100$ MPa and $Mo_6S_{4.5}I_{4.5}$ nanowires of $G = 900 \pm 150$ MPa are obtained. These results are summarized in Table 1. It is interesting to note that the MoS_xI_y nanotubes have the lowest shear modulus,[9] suggesting that the insertion of iodine into the lattice does vary the interaction between the nanotubes. On the other hand, it is puzzling to see that the Young's moduli of these new members seem to be higher than theoretical values. Our calculations give $E_Y \approx 110$ GPa for hypothetical structures with the C site occupied and a much lower value of ≈ 45 GPa for the experimental structure of $Mo_6S_3I_6$. We do not have a good explanation for this. Although the dispersion of the experimental points is high, presumably due to the fact that we are measuring bundles where the shear is very low, it seems that the E_Y values are beyond the scattering of the data points. As can be seen from Equation (2), for small-diameter bundles

Table 1. Results of nanomechanical measurements on $Mo_6S_3I_6$ and $Mo_6S_{4.5}I_{4.5}$ compared to MoS_2[9] and carbon nanotubes.[19]

Material	E_Y [GPa]	G [GPa]	Theoretical Young's modulus E_Y [Gpa]
$Mo_6S_3I_6$	430	0.45	45
$Mo_6S_{4.5}I_{4.5}$	420	0.89	-
MoS_2[9]	120	0.16	100
CNTs[19]	1000	1-10	900

the contribution of shearing is low and the bending modulus is close to the Young's modulus. For such thin bundles the values are already in the 400 GPa range.

These high measured values of E_Y are even more puzzling if we take into account that theoretical modeling can give the Young's modulus with high accuracy, in contrast to the shear modulus. In modeling, the shear is calculated as the difference between small quantities (tube–tube interaction), hence the error bar is large. The great advantage of our experimental technique is that, from a series of measurements performed on various bundle sizes, quantitative results for G can be obtained.

Our measurements show a marked difference in mechanical coupling between individual $Mo_6S_3I_6$ and $Mo_6S_{4.5}I_{4.5}$, indicating that they might be suited for different applications. This difference in mechanical coupling can be attributed to varying ratios of S and I atomic species on the nanowire surface. Due to lower values of G, $Mo_6S_3I_6$ might be better suited as a solid-state lubricant or lubricant additive. On the other hand, $Mo_6S_{4.5}I_{4.5}$, with its relatively higher G, would be more interesting for composite fabrication, as a higher shear modulus would ensure better mechanical coupling between wires and the composite matrix.

Experimental Section

Handpicked $Mo_6S_3I_6$ and $Mo_6S_{4.5}I_{4.5}$ material was dispersed in isopropyl alcohol using ultrasound for 15 min. The concentration was on the order of 10^{-2} mg mL^{-1}, expected to result in a mean bundle diameter of 10 nm.[30] Several drops of the solution were deposited on the surface of a polished alumina ultrafiltration membrane (Whatman anodisc) with a mean pore diameter of 200 nm. Samples were transferred into a Thermomicro M5 AFM, operating in air and equipped with capacitive displacement sensors and a closed-loop feedback for piezo scanner movement calibration and linearization, enabling accurate positioning. AFM imaging was performed in contact mode in air using Si_3N_4 cantilevers (Veeco Metrology) with nominal force constants between 0.03 and 0.1 N m^{-1}, calibrated by measuring their resonant frequency.[31] Resulting AFM topographical images recorded under a constant vertical force were analyzed using the SPIP software package (Image Metrology A/S). The effect of cantilever deflection was taken into account by measuring the height difference between the hard substrate (Al_2O_3 membrane) and the suspended bundle. Resulting linear bundle-deflection–force curves were fitted using the beam-bending model discussed above.

The same nanowire solution was used for the preparation of samples for TEM observation. Several drops of the solution were deposited on copper grids coated with lacey carbon and dried. TEM imaging was performed on a Philips CM-20 TEM operated at 200 kV.

Keywords:
atomic force microscopy · mechanical coupling · nanowires · shear modulus · Young's modulus

[1] S. Iijima, *Nature* **1991**, *354*, 56.
[2] N. G. Chopra, R. J. Luyken, K. Cherrey, V. H. Crespi, M. L. Cohen, S. G. Louie, A. Zettl, *Science* **1995**, *269*, 966.
[3] R. Tenne, L. Margulis, M. Genut, G. Hodes, *Nature* **1992**, *360*, 444.
[4] L. Margulis, G. Salitra, R. Tenne, M. Talianker, *Nature* **1993**, *365*, 113.
[5] M. Remskar, A. Mrzel, Z. Skraba, A. Jesih, M. Ceh, J. Demsar, P. Stadelmann, F. Levy, D. Mihailovic, *Science* **2001**, *292*, 479.
[6] D. Vrbanic, M. Remskar, A. Jesih, A. Mrzel, P. Umek, M. Ponikvar, B. Jancar, A. Meden, B. Novosel, S. Pejovnik, P. Venturini, J. C. Coleman, D. Mihailovic, *Nanotechnology* **2004**, *15*, 635.
[7] M. Sergent, O. Fischer, M. Decroux, C. Perrin, R. Chevrel, *J. Solid State Chem.* **1977**, *22*, 87.
[8] V. Nemanic, M. Zumer, B. Zajec, J. Pahor, M. Remskar, A. Mrzel, P. Panjan, D. Mihailovic, *Appl. Phys. Lett.* **2003**, *82*, 4573.
[9] A. Kis, D. Mihailovic, M. Remskar, A. Mrzel, A. Jesih, I. Piwonski, A. J. Kulik, W. Benoit, L. Forró, *Adv. Mater.* **2003**, *15*, 733.
[10] D. Mihailovic, Z. Jaglicic, D. Arcon, A. Mrzel, A. Zorko, M. Remskar, V. V. Kabanov, R. Dominko, M. Gaberscek, C. J. Gomez-Garcia, J. M. Martinez-Agudo, E. Coronado, *Phys. Rev. Lett.* **2003**, *90*, 146401.
[11] A. Zimina, S. Eisebitt, M. Freiwald, S. Cramm, W. Eberhardt, A. Mrzel, D. Mihailovic, *Nano Lett.* **2004**, *4*, 1749.
[12] I. Vilfan, D. Mihailovic, *Phys. Rev. B* **2006**, *74*, 235411.
[13] T. Yang, S. Okano, S. Berber, D. Tomanek, *Phys. Rev. Lett.* **2006**, *96*, 125502.
[14] A. Meden, A. Kodre, J. P. Gomilek, I. Aron, I. Vilfan, D. Vrbanic, A. Mrzel, D. Mihailovic, *Nanotechnology* **2005**, *16*, 1578.
[15] G. Paglia, E. S. Boin, D. Vengust, D. Mihailovic, S. J. L. Billinge, *Chem. Mater.* **2006**, *18*, 100.
[16] V. Nicolosi, P. D. Nellist, S. Sanvito, E. C. Cosgriff, S. Krishnamurthy, W. J. Blau, M. L. H. Green, D. Vengust, D. Dvorsek, D. Mihailovic, G. Compagnini, J. Sloan, V. Stolojan, J. D. Carey, S. J. Pennycook, J. N. Coleman, *Adv. Mater.* **2007**, *19*, 543.
[17] V. Nicolosi, D. Vrbanic, A. Mrzel, J. McCauley, S. O'Flaherty, D. Mihailovic, W. J. Blau, J. N. Coleman, *Chem. Phys. Lett.* **2005**, *401*, 13.
[18] R. G. Dickinson, L. Pauling, *J. Am. Chem. Soc.* **1923**, *45*, 1466.
[19] J.-P. Salvetat, G. A. D. Briggs, J.-M. Bonard, R. R. Bacsa, A. J. Kulik, T. Stöckli, N. Burnham, L. Forró, *Phys. Rev. Lett.* **1999**, *82*, 944.
[20] M. D. Segall, P. J. D. Lindan, M. J. Probert, C. J. Pickard, P. J. Hasnip, S. J. Clark, M. C. Payne, *J. Phys. Condens. Matter* **2002**, *14*, 2717.
[21] J. P. Perdew, K. Burke, M. Ernzerhof, *Phys. Rev. Lett.* **1996**, *77*, 3865.

[22] N. Marzari, D. Vanderbilt, M. C. Payne, *Phys. Rev. Lett.* **1997**, *79*, 1337.
[23] A. N. Kolmogorov, V. H. Crespi, *Phys. Rev. Lett.* **2000**, *85*, 4727.
[24] J.-P. Salvetat, A. J. Kulik, J.-M. Bonard, G. A. D. Briggs, T. Stöckli, K. Méténier, S. Bonnamy, F. Béguin, N. A. Burnham, L. Forró, *Adv. Mater.* **1999**, *11*, 161.
[25] B. Lukic, J. W. Seo, E. Couteau, K. Lee, S. Gradecak, R. Berkecz, K. Hernadi, S. Delpeux, T. Cacciaguerra, F. Béguin, A. Fonseca, J. B. Nagy, G. Csányi, A. Kis, A. J. Kulik, L. Forró, *Appl. Phys. A* **2005**, *80*, 695.
[26] A. Kis, G. Csanyi, J.-P. Salvetat, T.-N. Lee, E. Couteau, A. J. Kulik, W. Benoit, J. Brugger, L. Forró, *Nat. Mater.* **2004**, *3*, 153.
[27] A. Kis, S. Kasas, B. Babic, A. J. Kulik, W. Benoît, G. A. D. Briggs, C. Schönenberger, S. Catsicas, L. Forró, *Phys. Rev. Lett.* **2002**, *89*, 248101.
[28] H. Ni, X. Li, H. Gao, *Appl. Phys. Lett.* **2006**, *88*, 043108.
[29] J. M. Gere, S. P. Timoshenko, *Mechanics of Materials*, PWS-Kent, Boston, **1984**.
[30] V. Nicolosi, D. Vengust, D. Mihailovic, W. J. Blau, J. N. Coleman, *Chem. Phys. Lett.* **2006**, *425*, 89.
[31] J. P. Cleveland, S. Manne, D. Bocek, P. K. Hansma, *Rev. Sci. Instrum.* **1993**, *64*, 403.

Received: March 7, 2007
Published online on August 20, 2007

